

S1 Additional Figures

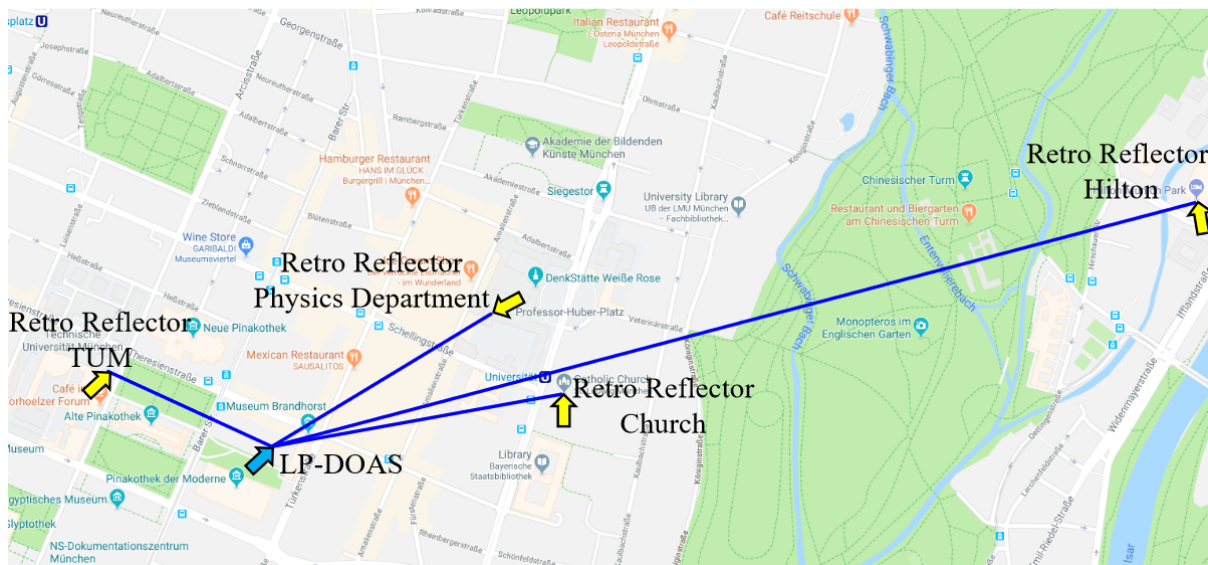


Figure S1. The setup of the LP-DOAS system on the MIM's rooftop with its four optical paths towards TUM N5 building, LMU physics building and Hilton hotel (Figure from Zhu et al., 2020). The retro reflector at the Church was only installed in January 2017 and was not available in 2016 during the MuNIC campaign. Map data (c)Google maps.

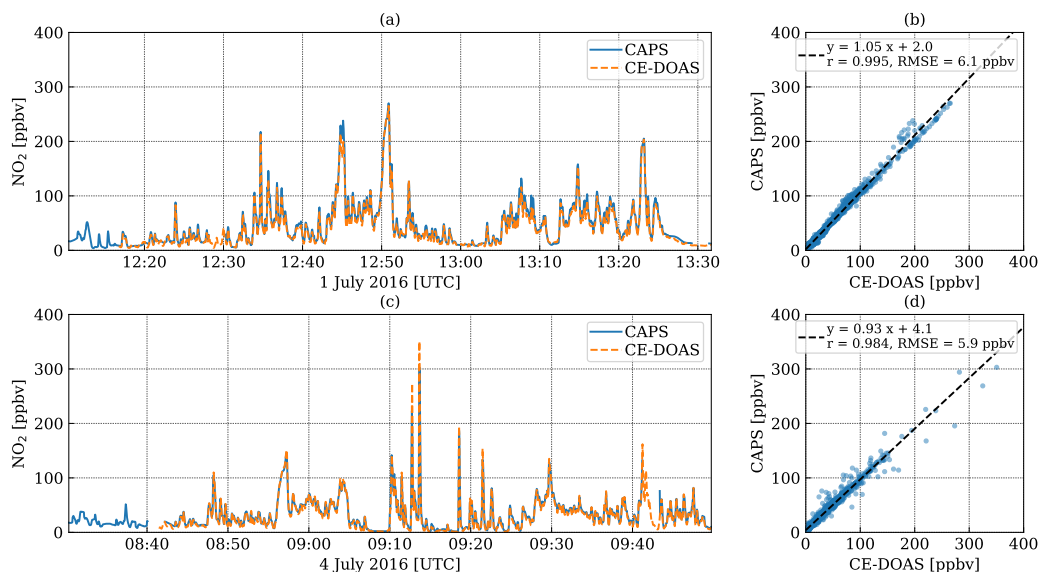


Figure S2. (a,c) Time series of NO_2 concentrations measured by CAPS and CE-DOAS on 1 and 4 July 2016 on-board the LMU vehicle. (b,c) Scatter plots comparing CAPS and CE-DOAS.

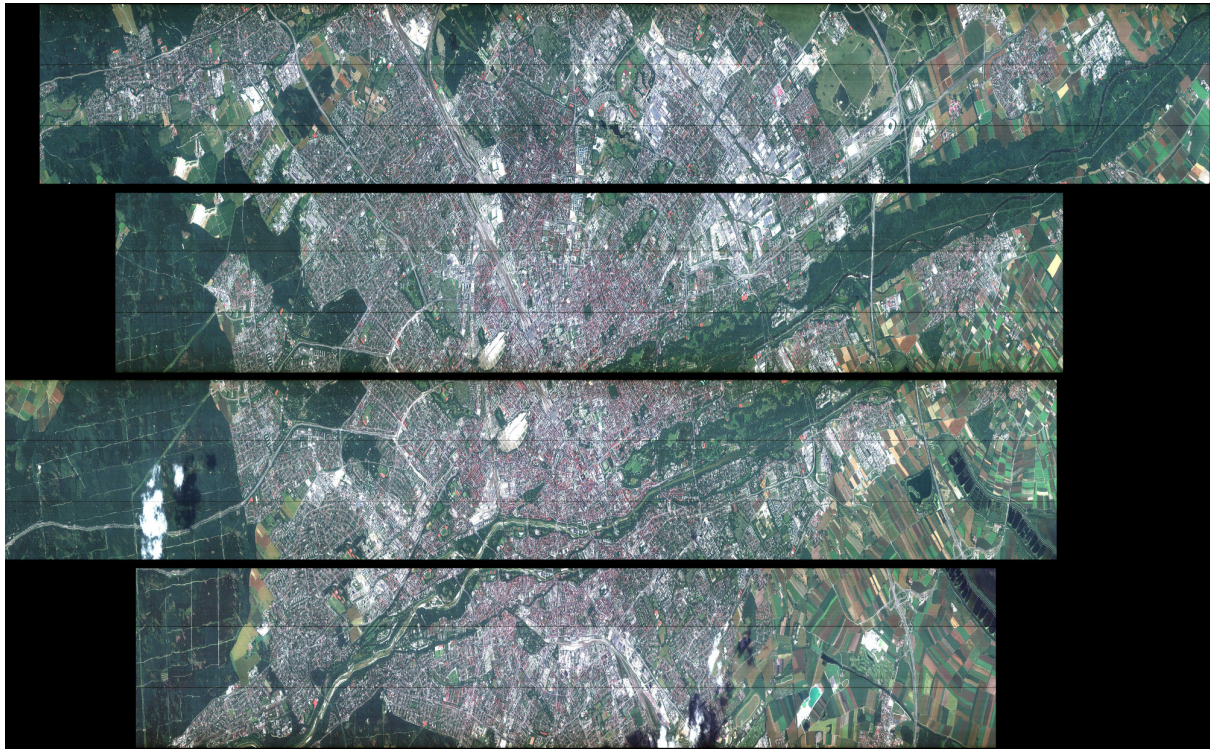


Figure S3. True color composite of the four APEX stripes (#1 to #4 from bottom to top) measured during the MuNIC campaign.

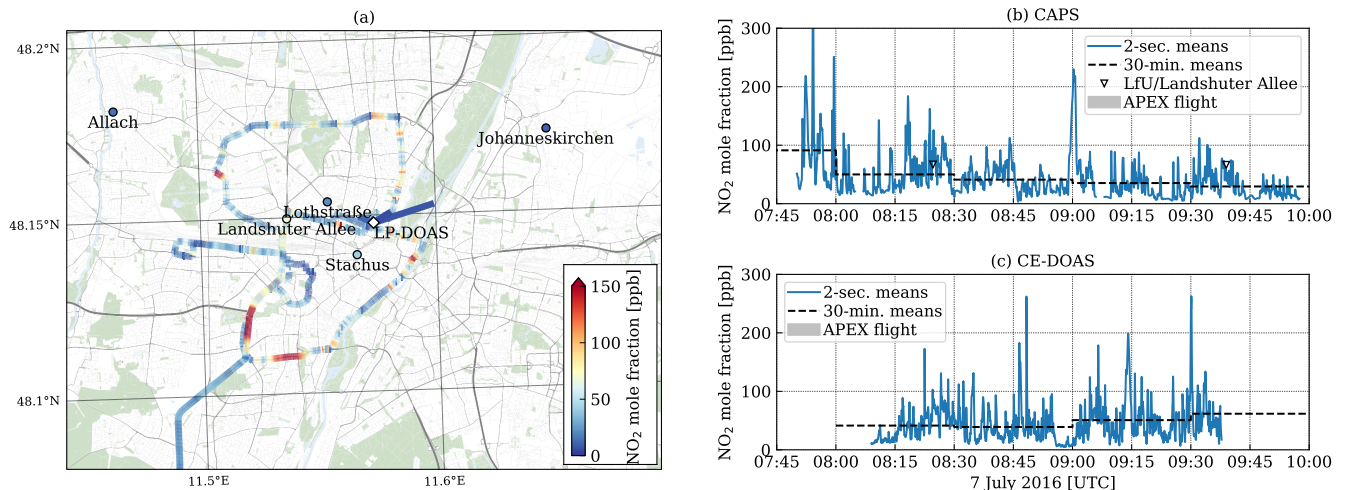


Figure S4. (a) Map of NO₂ mole fractions measured by LMU and MPIC cars in the morning. (b) and (c) show the time series of NO₂ mole fractions measured by the CAPS and CE-DOAS instrument on the LMU and MPIC car, respectively. Map data from © OpenStreetMap contributors 2021. Distributed under the Open Data Commons Open Database License (ODbL) v1.0.

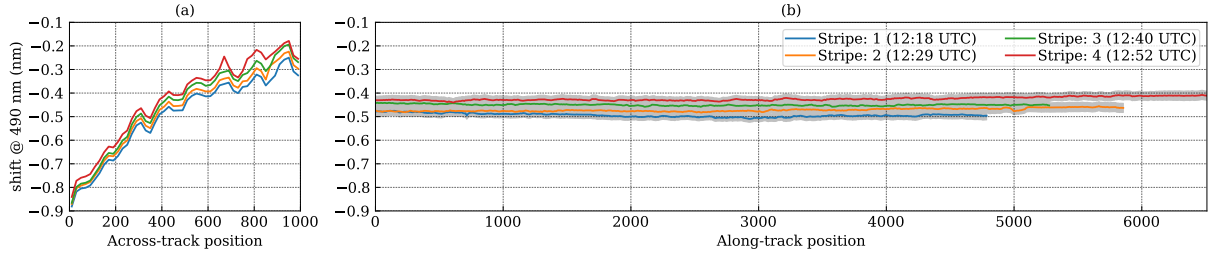


Figure S5. Mean (a) across- and (b) along-track shift of center wavelength at 490 nm after in-flight calibration for the four APEX stripes. Gray area shows standard error for all across- and along-track pixels.

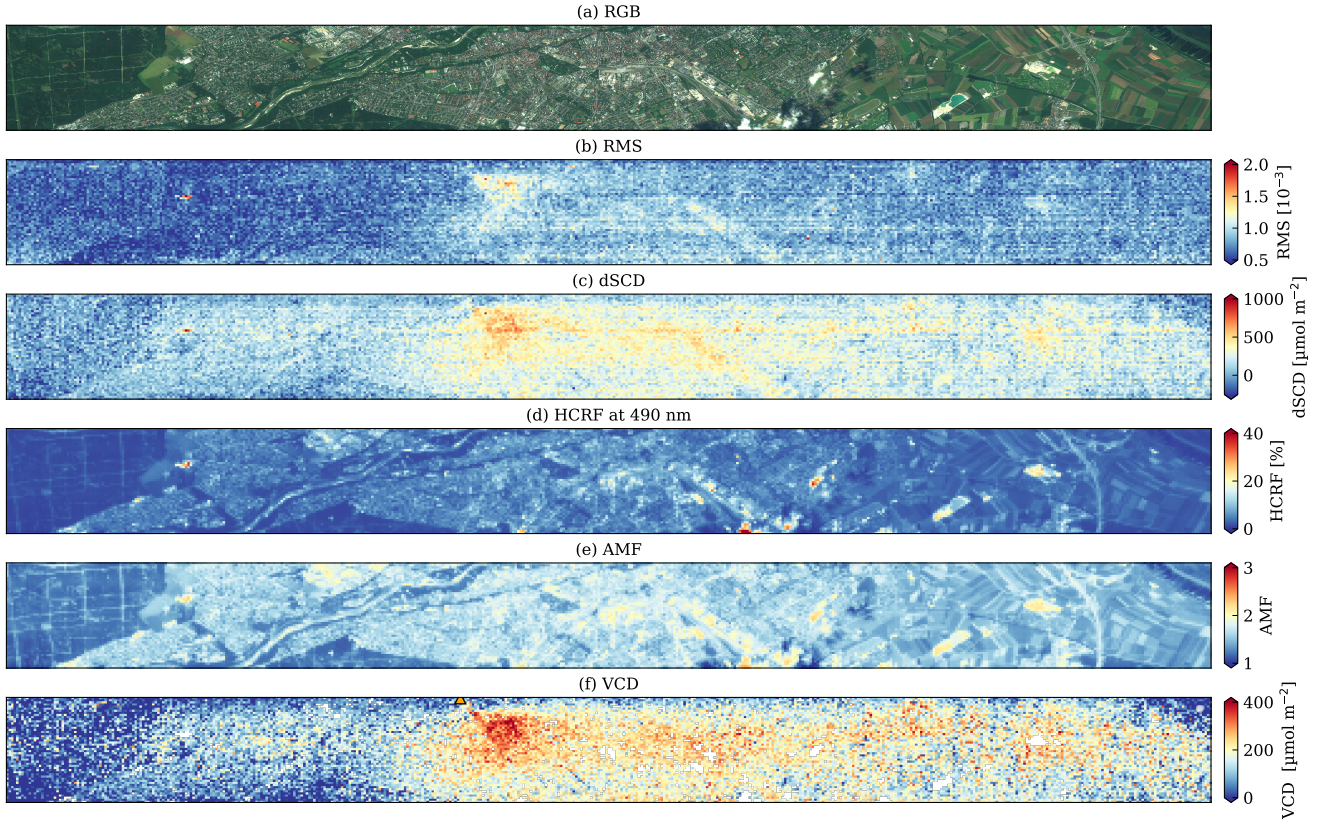


Figure S6. APEX stripe #1: (a) True color image, (b) Root mean square (RMS), (c) NO₂ differential slant column densities (dSCD), (d) hemispheric-conical reflectance factors (HCRF), (e) air mass factors (AMF) and (f) NO₂ vertical column densities (VCD).

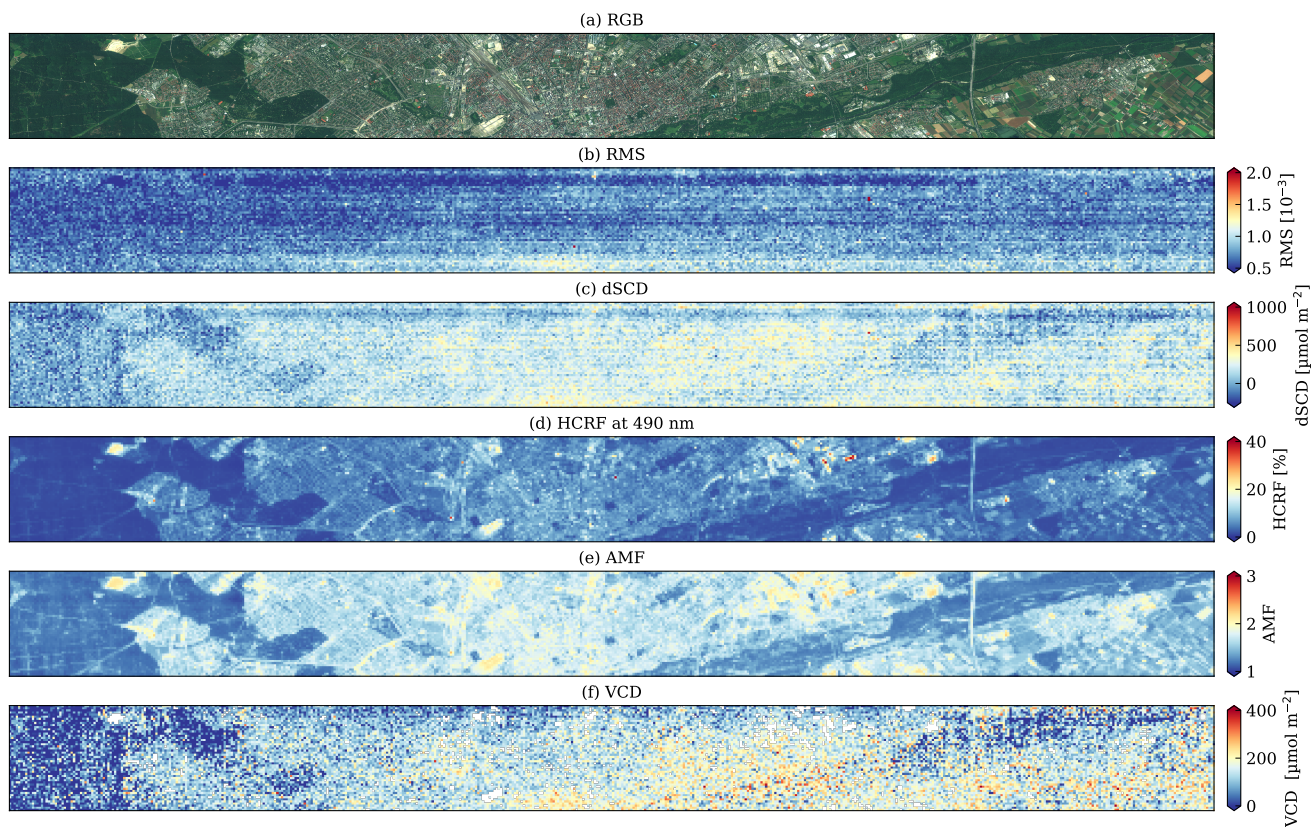


Figure S7. APEX stripe #3: (a) True color image, (b) Root mean square (RMS), (c) NO₂ differential slant column densities (dSCD), (d) hemispheric-conical reflectance factors (HCRF), (e) air mass factors (AMF) and (f) NO₂ vertical column densities (VCD).

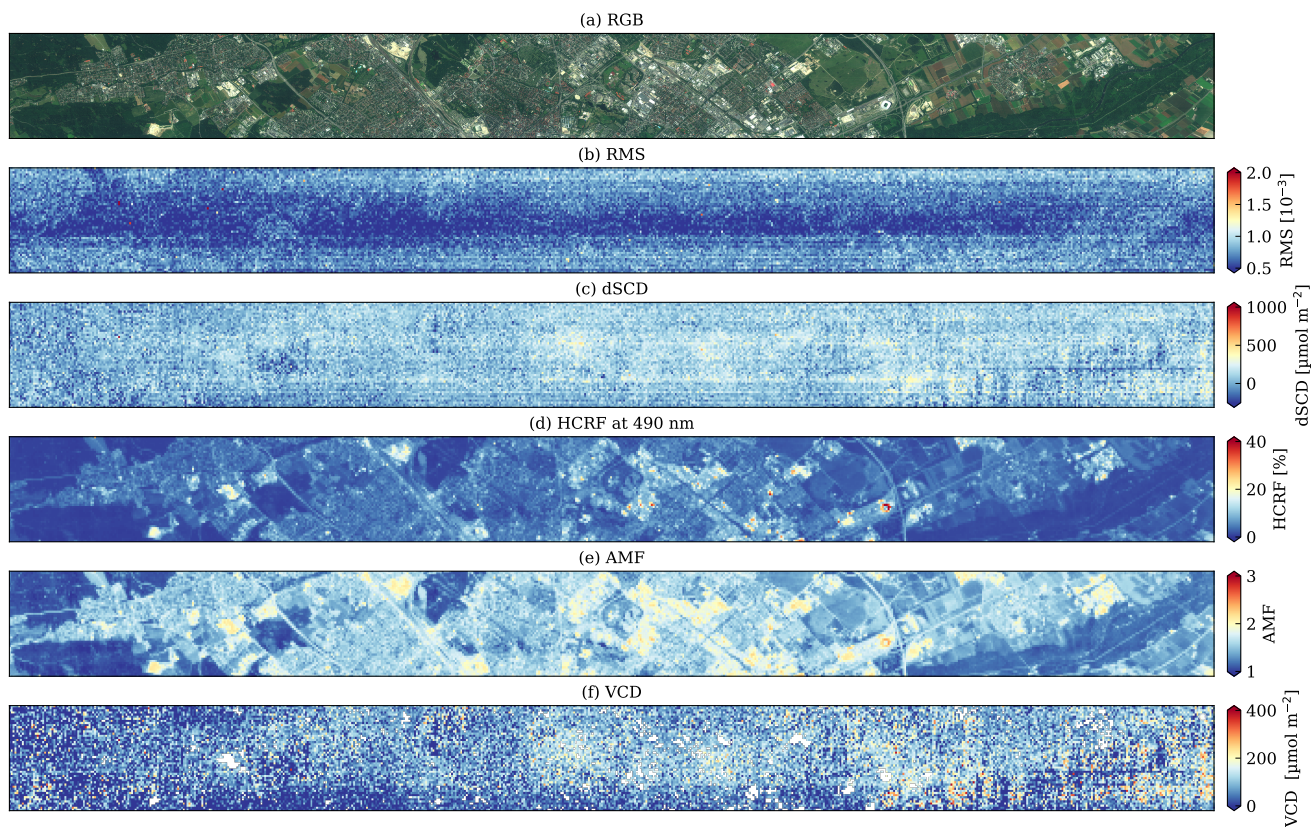


Figure S8. APEX stripe #4: (a) True color image, (b) Root mean square (RMS), (c) NO₂ differential slant column densities (dSCD), (d) hemispheric-conical reflectance factors (HCRF), (e) air mass factors (AMF) and (f) NO₂ vertical column densities (VCD).

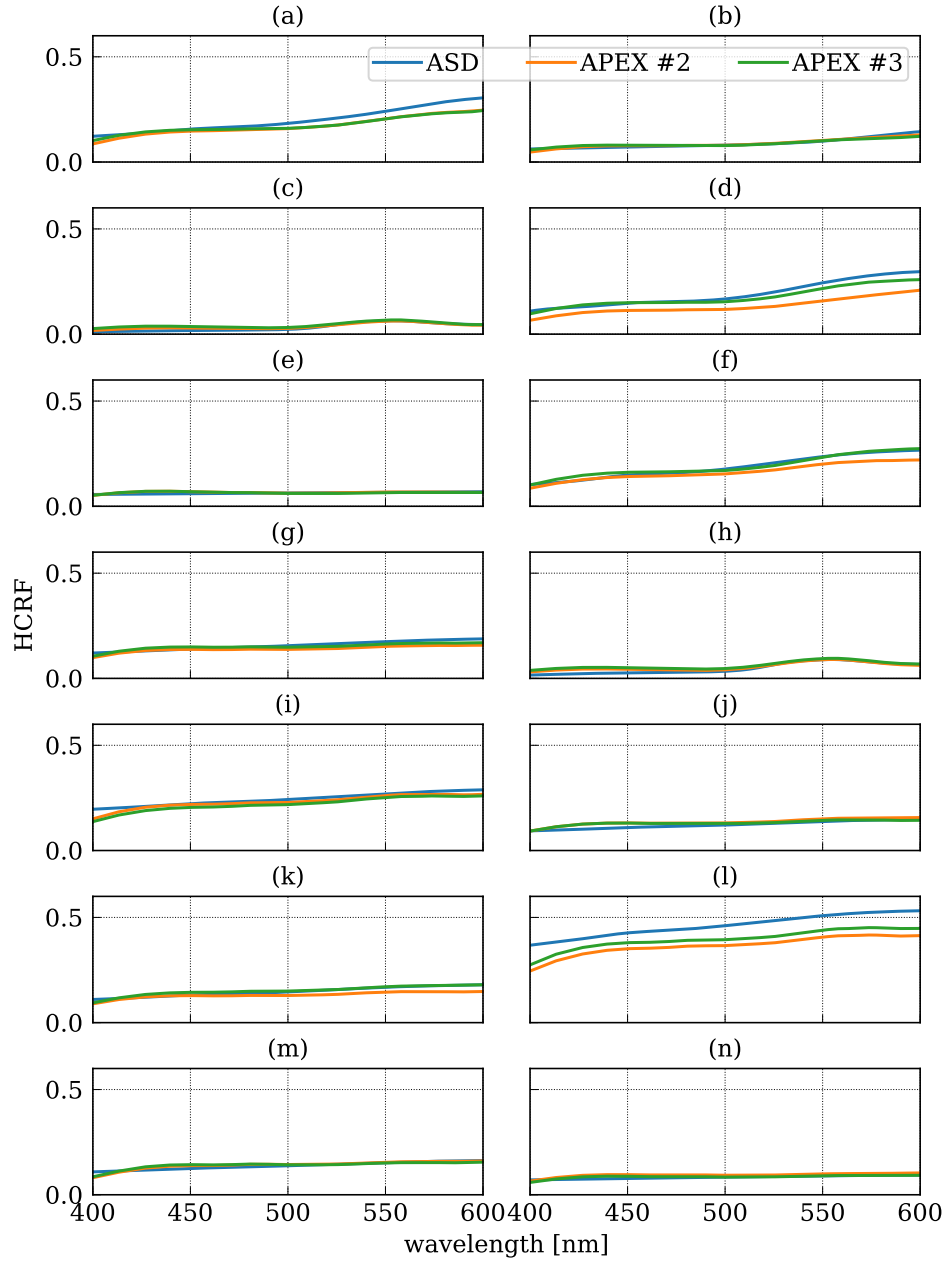


Figure S9. Comparison of APEX and ASD Hemispheric-conic reflectance factors (HCRF). The location of APEX and ASD measurements are shown in Table S1.

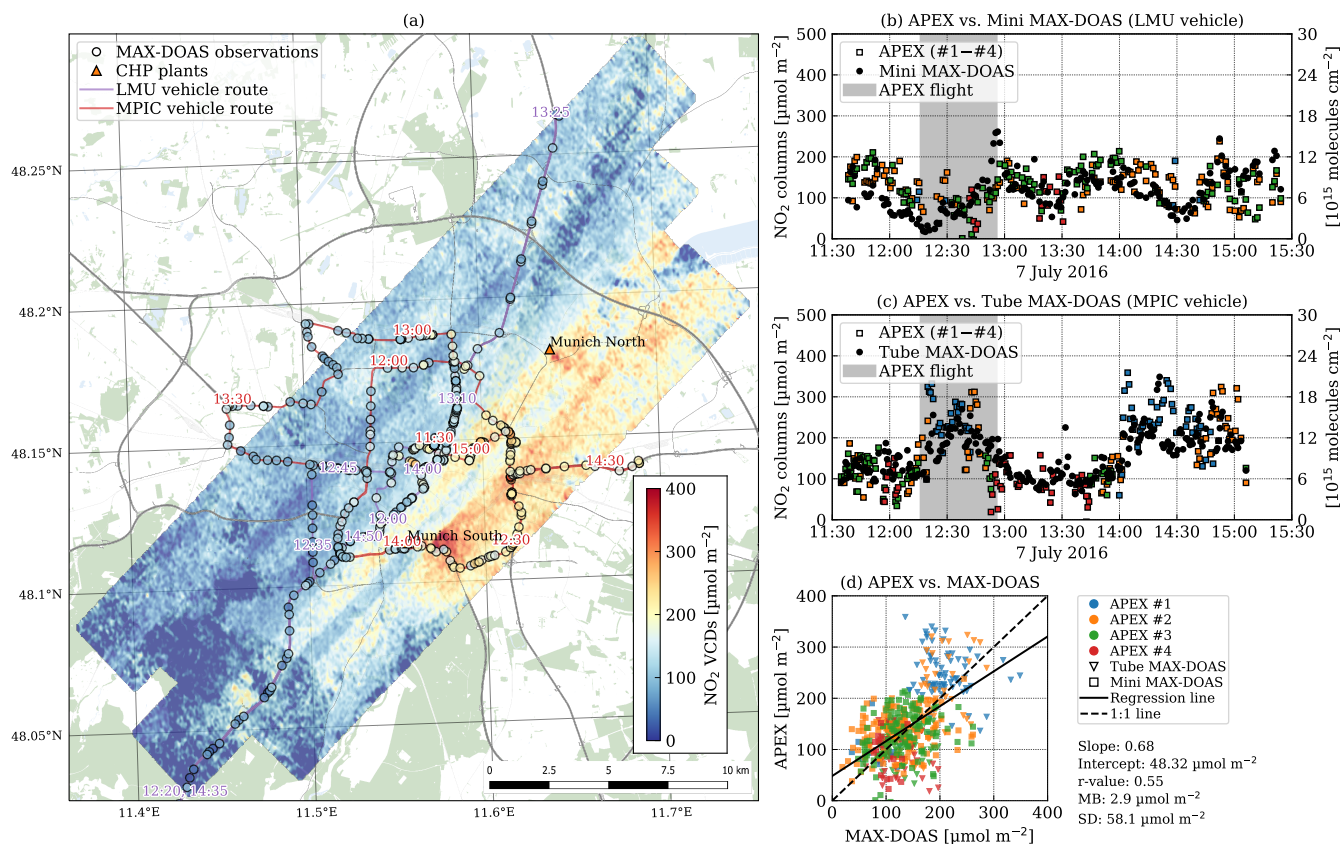


Figure S10. (a) Map NO₂ VCDs from APEX and mobile MAX-DOAS measurements on 7 July 2016 (afternoon) and time labels. (b,c) Time series of spatially co-located APEX and (b) Mini MAX-DOAS and (c) Tube MAX-DOAS VCDs. (d) Scatter plot showing MAX-DOAS and APEX NO₂ VCDs for spatially co-located observations. Map data from © OpenStreetMap contributors 2021. Distributed under the Open Data Commons Open Database License (ODbL) v1.0.

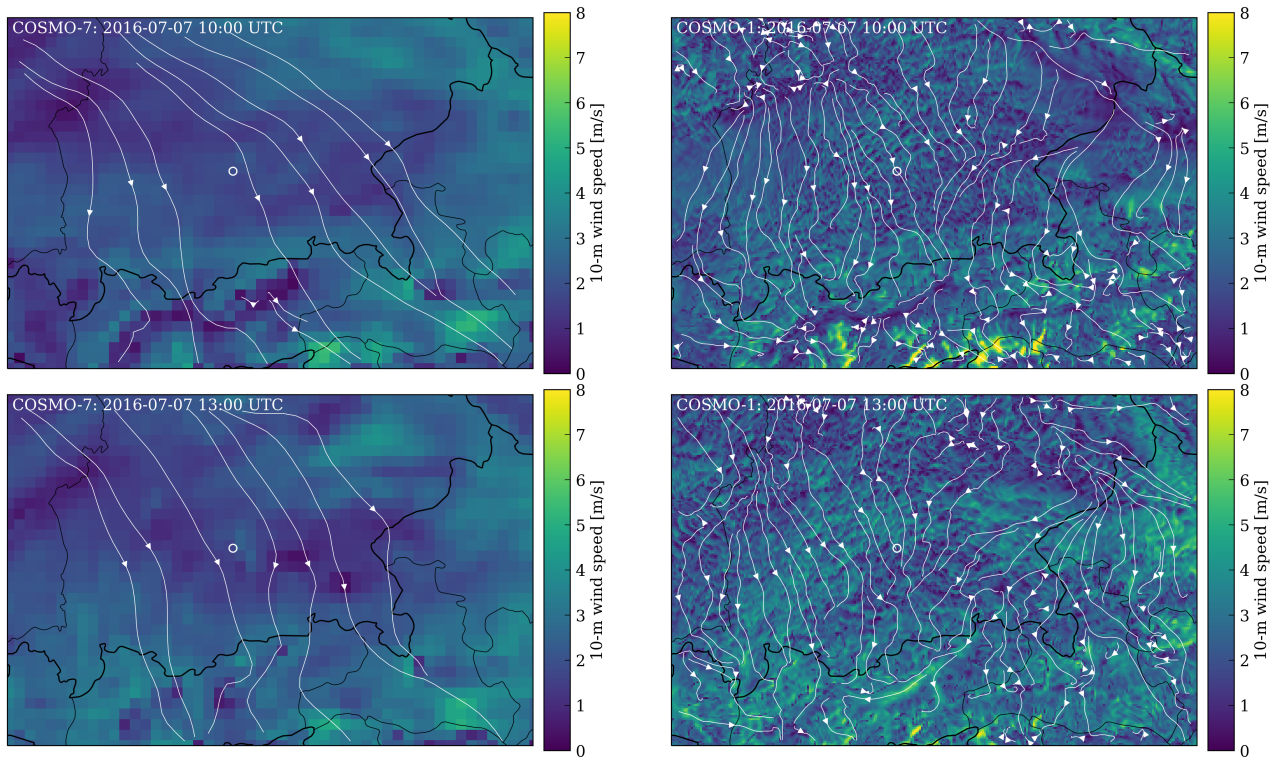


Figure S11. Maps of 10-m wind speeds at 10 and 13 UTC from the COSMO-7 and COSMO-1 model with 7 km and 1 km spatial resolution. The COSMO-1 model shows highly variable 10-m wind speeds over Munich with a similar spatial variability as the ground measurements. Since the COSMO-7 model does not resolve the convective cells at 7 km resolution, 10-m wind speeds vary spatially less.

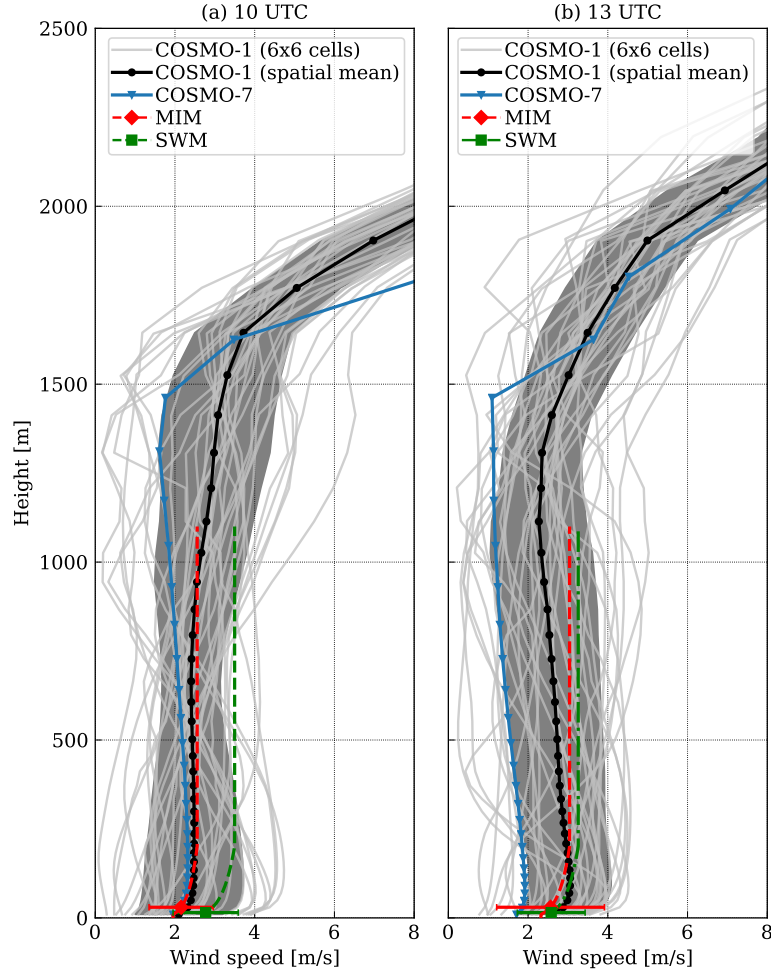


Figure S12. Wind profiles at (a) 10 UTC and (b) 13 UTC at Munich South CHP plant from the COSMO-1 and COSMO-7 model. COSMO-1 profiles are shown for 6×6 grid cells and as spatial mean with standard deviation. In addition, wind profiles were extrapolated from wind measurements at the MIM's rooftop and at the plant site provided by Stadtwerke München (SWM) using the empirical equations recommended by the Association of German Engineers (VDI - Fachbereich Umweltmeteorologie, 1985, 2009). At noon (10 UTC), the COSMO-1 and COSMO-7 analysis product agree quite well, but individual COSMO-1 profiles show very high variability within 6×6 grid cells. The wind profiles extrapolated from measurements also agree with the simulated wind fields. In the afternoon (13 UTC), COSMO-1 winds increased by about 1 m s^{-1} , while COSMO-7 winds remain similar to the noon values.

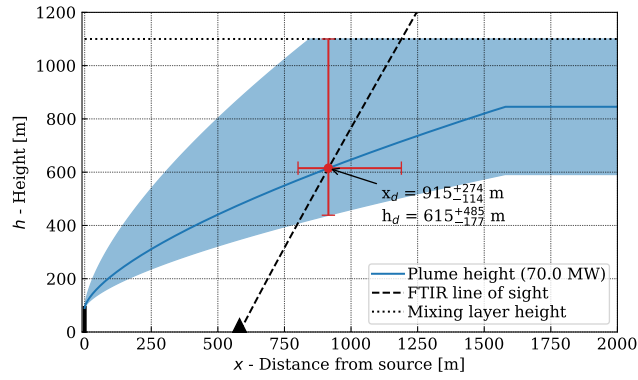


Figure S13. Plume rise of emission plume of Munich South CHP plant assuming heat emissions of 70 MW using VDI guidelines. The plume height and the line-of-sight of the FTIR spectrometer intersect at about $x_d = 918$ m downstream of the source at $h_d = 620$ m above ground. The uncertainty is obtained from the uncertainty of the wind speed at the stack ($2.5 \pm 1.2 \text{ m s}^{-1}$).

S2 Additional Tables

Table S1. Name and locations of APEX and ASD reflectance spectra. Indices in APEX stripes #2 and #3 are shown.

#	Surface type	Location	Longitude	Latitude	APEX index (#2)		APEX index (#3)	
			[°E]	[°N]	across	along	across	along
1	Sand	Sports ground	11.5245	48.1268	30	3373	381	1822
2	Cinder track	Sports ground	11.5240	48.1270	22	3387	391	1813
3	Lawn	Sports ground	11.5239	48.1264	35	3384	377	1811
4	Tartan track	Westpark	11.5398	48.1286	224	3174	187	1979
5	Dark asphalt	Westpark	11.5410	48.1284	238	3165	165	1985
6	Bright gravel	Westpark	11.5408	48.1283	243	3169	167	1981
7	Bright asphalt	Theresienwiese	11.5526	48.1312	349	2992	60	2123
8	Lawn	Koenigsplatz	11.5658	48.1452	209	2646	200	2460
9	Gravel	Koenigsplatz	11.5651	48.1455	188	2647	220	2460
10	Cobblestones	Koenigsplatz	11.5649	48.1460	169	2649	233	2462
11	Bright cobblestones	Koenigsplatz	11.5642	48.1463	155	2644	249	2457
12	Bright paving stone	Koenigsplatz	11.5674	48.1454	226	2623	186	2477
13	Paving stone	LMU main building	11.5816	48.1507	301	2378	100	2683
14	Dark cobblestones	Siegestor	11.5821	48.1522	275	2353	129	2711

Table S2. Input and output parameter from emission quantification of NO_x emissions with distance from source L , effective plume height h_d , wind speed in plume u , angle between wind centerline and APEX stripe α , residence time τ , NO₂-to-NO_x conversion factor f , estimated emissions Q as well as standard width σ and location μ of Gaussian curve.

Stripe	Source	Box	L [m]	h_d [m]	u [m s ⁻¹]	α [deg]	τ [s]	f	Q [kg s ⁻¹]	σ [m]	μ [m]
#1	M. South	1	342.4	279.7	3.2±1.3	34±5	108.1	10.5±6.3	26.7±19.8	43±8	-14±9
#1	M. South	2	820.9	430.0	2.9±1.2	41±5	282.6	4.3±2.4	80.0±55.1	398±37	-447±39
#1	M. South	3	1364.3	567.0	2.7±1.0	49±5	500.4	2.7±1.4	48.9±31.3	374±29	-63±36
#2	M. South	1	398.4	306.9	3.0±1.3	46±5	131.0	8.8±5.3	115.9±85.0	240±17	-88±22
#2	M. South	2	851.4	450.0	2.8±1.1	38±5	298.9	4.1±2.3	51.6±35.6	154±9	170±10
#2	M. North	1	213.2	232.9	3.5±0.9	1±5	61.4	18.1±9.6	106.7±65.9	190±35	-1±33
#2	M. North	2	554.1	360.2	3.5±1.0	6±5	157.7	7.4±4.0	43.2±27.1	131±20	60±19
#2	M. North	3	916.7	468.1	3.6±1.2	12±5	256.8	4.7±2.5	54.6±35.6	460±84	-266±73

Table S3. Input and output parameter from emission quantification of CO₂ emissions with differential column measurement (DCM), wind speed at stack u_{stack} , distance from stack x_d , height of plume h_d , wind speed inside plume u_{plume} , dispersion coefficient σ_y and estimated CO₂ emissions Q .

Peak	UTC	DCM [kg m ⁻²]	u_{stack} [m s ⁻¹]	x_d [m]	h_d [m]	u_{plume} [m s ⁻¹]	σ_y [m]	Q [kg s ⁻¹]
1	09:47	0.068	2.5±1.1	918 ⁺²⁷¹ ₋₁₁₀	621 ⁺⁴⁶³ ₋₁₆₉	2.3 ± 0.7	318 ⁺⁸⁴ ₋₃₅	124.2 ± 46.8
2	09:48	0.028	2.5±1.1	918 ⁺²⁷¹ ₋₁₁₀	621 ⁺⁴⁶⁷ ₋₁₆₉	2.3 ± 0.7	318 ⁺⁸⁴ ₋₃₅	51.0 ± 23.6
3	09:48	0.043	2.5±1.2	918 ⁺²⁷¹ ₋₁₁₀	621 ⁺⁴⁷¹ ₋₁₇₀	2.3 ± 0.7	318 ⁺⁸⁴ ₋₃₅	79.2 ± 32.0
4	09:51	0.035	2.5±1.2	918 ⁺²⁷¹ ₋₁₁₂	620 ⁺⁴⁸⁰ ₋₁₇₂	2.3 ± 0.7	318 ⁺⁸⁴ ₋₃₅	64.9 ± 27.8
5	09:57	0.070	2.5±1.2	918 ⁺²⁷¹ ₋₁₁₅	620 ⁺⁴⁸⁰ ₋₁₇₇	2.4 ± 0.7	318 ⁺⁸⁴ ₋₃₆	131.8 ± 49.9
6	10:00	0.035	2.5±1.3	918 ⁺²⁷¹ ₋₁₁₇	620 ⁺⁴⁸⁰ ₋₁₇₉	2.4 ± 0.7	318 ⁺⁸⁴ ₋₃₇	67.1 ± 28.9
7	10:01	0.070	2.5±1.3	915 ⁺²⁷⁴ ₋₁₁₄	615 ⁺⁴⁸⁵ ₋₁₇₇	2.4 ± 0.7	317 ⁺⁸⁵ ₋₃₆	134.4 ± 51.3
8	10:11	0.049	2.6±1.3	903 ⁺²⁸⁶ ₋₁₀₇	594 ⁺⁴⁸⁷ ₋₁₆₆	2.4 ± 0.8	313 ⁺⁸⁸ ₋₃₄	91.0 ± 38.2
9	10:17	0.032	2.6±1.3	896 ⁺²⁹³ ₋₁₀₃	581 ⁺⁴⁵⁴ ₋₁₅₉	2.4 ± 0.8	311 ⁺⁹¹ ₋₃₂	58.0 ± 27.6
10	10:28	0.047	2.7±1.3	884 ⁺³⁰⁵ ₋₉₅	559 ⁺⁴⁰⁷ ₋₁₄₉	2.3 ± 0.9	307 ⁺⁹⁴ ₋₃₀	85.0 ± 39.2
11	10:44	0.039	2.8±1.3	869 ⁺²⁹³ ₋₈₇	532 ⁺³⁵¹ ₋₁₃₅	2.3 ± 1.0	302 ⁺⁹¹ ₋₂₇	69.1 ± 34.8
12	10:48	0.045	2.9±1.3	865 ⁺²⁷⁸ ₋₈₄	525 ⁺³³⁷ ₋₁₃₂	2.3 ± 1.0	301 ⁺⁸⁶ ₋₂₇	78.7 ± 39.2
13	10:55	0.065	2.9±1.3	859 ⁺²⁵⁹ ₋₈₁	514 ⁺³¹⁸ ₋₁₂₇	2.3 ± 1.0	299 ⁺⁸⁰ ₋₂₆	114.6 ± 55.8
14	11:09	0.021	3.1±1.3	844 ⁺²¹⁶ ₋₇₃	487 ⁺²⁷⁴ ₋₁₁₅	2.5 ± 1.1	295 ⁺⁶⁷ ₋₂₃	37.8 ± 22.9
15	11:19	0.051	3.2±1.3	833 ⁺¹⁸⁹ ₋₆₇	468 ⁺²⁴⁶ ₋₁₀₇	2.6 ± 1.1	291 ⁺⁵⁹ ₋₂₁	97.0 ± 46.0
16	11:30	0.030	3.4±1.3	823 ⁺¹⁶⁵ ₋₆₂	449 ⁺²²⁰ ₋₉₉	2.7 ± 1.1	288 ⁺⁵² ₋₂₀	58.7 ± 30.1
17	11:34	0.040	3.4±1.3	819 ⁺¹⁵⁸ ₋₅₉	443 ⁺²¹² ₋₉₆	2.8 ± 1.1	287 ⁺⁵⁰ ₋₁₉	80.0 ± 38.1
18	11:47	0.019	3.6±1.3	809 ⁺¹³⁸ ₋₅₅	424 ⁺¹⁸⁹ ₋₈₉	2.9 ± 1.2	284 ⁺⁴³ ₋₁₇	38.7 ± 23.5

References

- VDI - Fachbereich Umweltmeteorologie: Dispersion of air pollutants in the atmosphere; determination of plume rise, Tech. Rep. VDI 3782 Blatt 3, VDI/DIN-Kommission Reinhaltung der Luft (KRdL) - Normenausschuss, 1985.
- 5 VDI - Fachbereich Umweltmeteorologie: Atmospheric dispersion models; Gaussian plume model for the determination of ambient air characteristics, Tech. Rep. VDI 3782 Blatt 1, VDI/DIN-Kommission Reinhaltung der Luft (KRdL) - Normenausschuss, 2009.
- 10 Zhu, Y., Chen, J., Bi, X., Kuhlmann, G., Chan, K. L., Dietrich, F., Brunner, D., Ye, S., and Wenig, M.: Spatial and temporal representativeness of point measurements for nitrogen dioxide pollution levels in cities, *Atmospheric Chemistry and Physics*, 20, 13 241–13 251, <https://doi.org/10.5194/acp-20-13241-2020>, 2020.